An Experimental Study of Blood Oxygen Saturation Imaging via Quantitative Photoacoustic Tomography

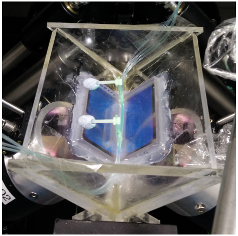

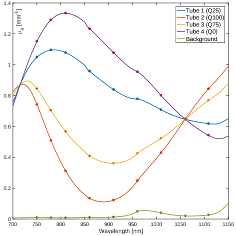

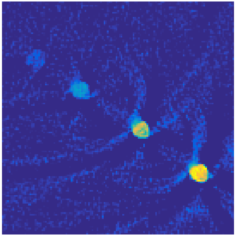

Felix Lucka, University College London, f.lucka@ulc.ac.uk

joint odyssey with: Lu An, Simon Arridge, Paul Beard, Ben Cox, Robert Ellwood, Martina Bargeman Fonseca & Emma Malone.

Centre for Medical Image Computing

(Very) Applied Inverse Problems
Hangzhou, June 2, 2017.

UCL CENTRE FOR INVERSE PROBLEMS

Optical Part

chromophore concentration: c_k

optical absorption coefficient: $\mu_a(c)$

Acoustic Part

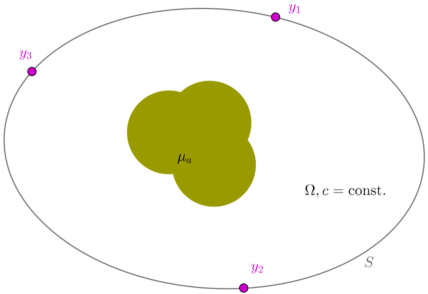

Photoacoustic Imaging: Basic Principles

Optical Part

chromophore concentration: c_k

optical absorption coefficient: $\mu_a(c)$

pulsed laser excitation: $\Phi(\mu_a)$

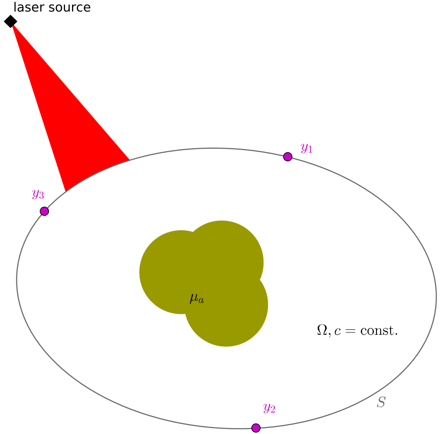

Acoustic Part

Optical Part

chromophore concentration: c_k

optical absorption coefficient: $\mu_a(c)$

pulsed laser excitation: $\Phi(\mu_a)$

thermalization: $H = \mu_a \Phi(\mu_a)$

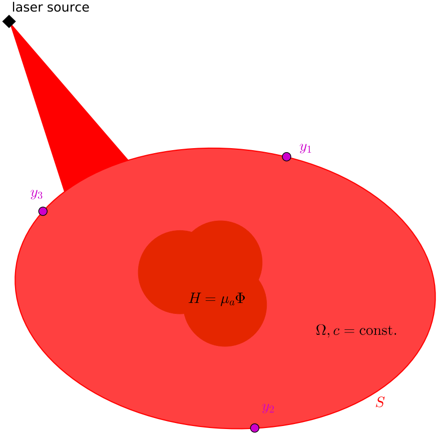

Acoustic Part

Optical Part

chromophore concentration: c_k

optical absorption coefficient: $\mu_a(c)$

pulsed laser excitation: $\Phi(\mu_a)$

thermalization: $H = \mu_a \Phi(\mu_a)$

Acoustic Part

local pressure increase: $p_0 = \Gamma(c) H$

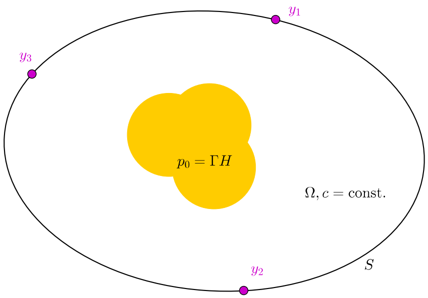

Photoacoustic Imaging: Basic Principles

Optical Part

chromophore concentration: c_k

optical absorption coefficient: $\mu_a(c)$

pulsed laser excitation: $\Phi(\mu_a)$

thermalization: $H = \mu_a \Phi(\mu_a)$

Acoustic Part

local pressure increase: $p_0 = \Gamma(c) H$

elastic wave propagation:

$$\Delta p - \frac{1}{c^2} \frac{\partial^2 p}{\partial^2 t} = 0$$

$$p|_{t=0} = p_0, \quad \frac{\partial p}{\partial t}|_{t=0} = 0$$

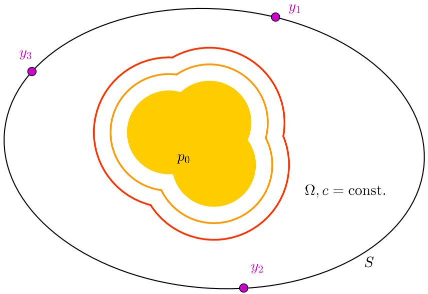

Optical Part

chromophore concentration: c_k

optical absorption coefficient: $\mu_a(c)$

pulsed laser excitation: $\Phi(\mu_a)$

thermalization: $H = \mu_a \Phi(\mu_a)$

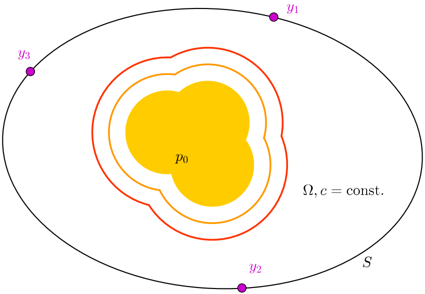

Acoustic Part

local pressure increase: $p_0 = \Gamma(c) H$

elastic wave propagation:

$$\Delta p - \frac{1}{c^2}\frac{\partial^2 p}{\partial^2 t} = 0$$

$$p|_{t=0} = p_0, \quad \frac{\partial p}{\partial t}|_{t=0} = 0$$

measurement of pressure time courses:

$$f_i(t) = p(y_i, t)$$

Photoacoustic Imaging: Basic Principles

Optical Part

chromophore concentration: c_k

optical absorption coefficient: $\mu_a(c)$

pulsed laser excitation: $\Phi(\mu_a)$

thermalization: $H = \mu_a \Phi(\mu_a)$

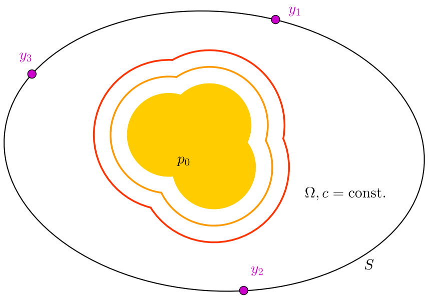

Acoustic Part

local pressure increase: $p_0 = \Gamma(c)H$

elastic wave propagation:

$$\Delta p - \frac{1}{c^2}\frac{\partial^2 p}{\partial^2 t} = 0$$

$$p|_{t=0} = p_0, \quad \frac{\partial p}{\partial t}|_{t=0} = 0$$

measurement of pressure time courses:

$$f_i(t) = p(y_i, t)$$

Photoacoustic effect

- coupling of optical and acoustic modalities.
- "hybrid imaging"
- high optical contrast can be read by high-resolution ultrasound.

Optical Part

chromophore concentration: c_k

optical absorption coefficient: $\mu_a(c)$

pulsed laser excitation: $\Phi(\mu_a)$

thermalization: $H = \mu_a \Phi(\mu_a)$

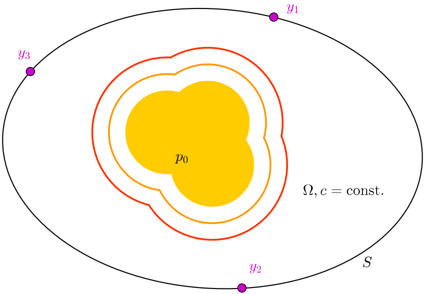

Acoustic Part

local pressure increase: $p_0 = \Gamma(c)H$

elastic wave propagation:

$$\Delta p - \frac{1}{c^2}\frac{\partial^2 p}{\partial^2 t} = 0$$

$$p|_{t=0} = p_0, \quad \frac{\partial p}{\partial t}|_{t=0} = 0$$

measurement of pressure time courses:

$$f_i(t) = p(y_i, t)$$

Inverse problems:

! optical inversion (μ_a) from boundary data: severely ill-posed.

Photoacoustic Imaging: Basic Principles

Optical Part

chromophore concentration: c_k

optical absorption coefficient: $\mu_a(c)$

pulsed laser excitation: $\Phi(\mu_a)$

thermalization: $H = \mu_a \Phi(\mu_a)$

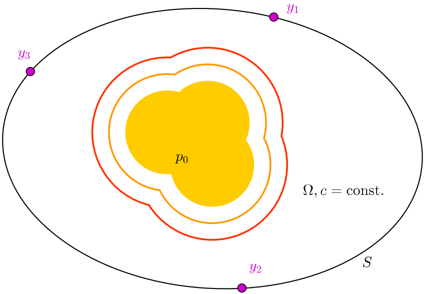

Acoustic Part

local pressure increase: $p_0 = \Gamma(c)H$

elastic wave propagation:

$$\Delta p - \frac{1}{c^2}\frac{\partial^2 p}{\partial^2 t} = 0$$

$$p|_{t=0} = p_0, \quad \frac{\partial p}{\partial t}|_{t=0} = 0$$

measurement of pressure time courses:

$$f_i(t) = p(y_i, t)$$

Inverse problems:

! optical inversion (μ_a) from boundary data: severely ill-posed.

✓ acoustic inversion (p_0) from boundary data: moderately ill-posed.

✓ optical inversion (μ_a) from internal data: moderately ill-posed.

Photoacoustic Imaging: Applications & Properties

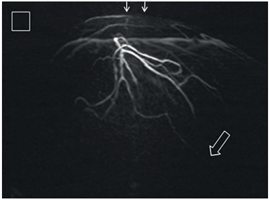

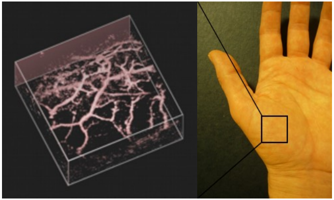

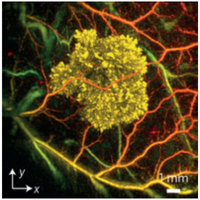

- Light-absorbing structures in soft tissue.
- High contrast between blood and water/lipid.
- 3D spatial resolutions of tens of micro meters.

sources: Paul Beard, 2011; Jathoul et al., 2015.

Photoacoustic Imaging: Spectral Properties

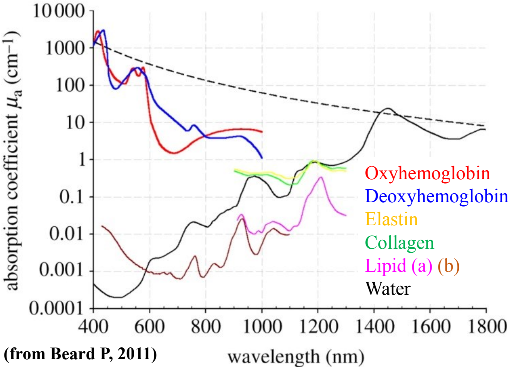

(from Beard P, 2011)

- Different wavelengths allow quantitative spectroscopic examinations.
- Gap between oxygenated and deoxygenated blood.
- Use of contrast agents for molecular imaging.

sources: Paul Beard, 2011; Jathoul et al., 2015.

Photoacoustic Imaging: Spectral Properties

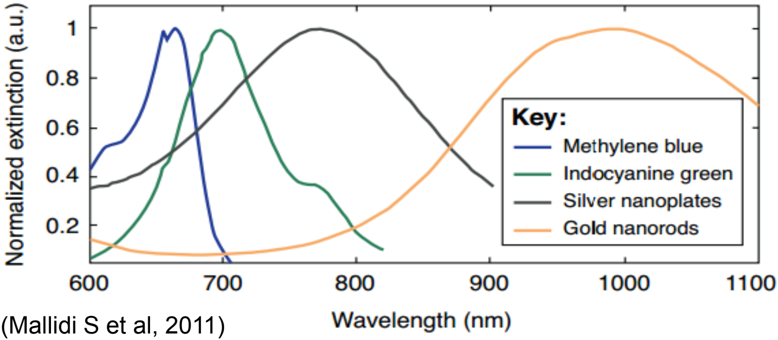

(Mallidi S et al, 2011)

- Different wavelengths allow quantitative spectroscopic examinations.
- Gap between oxygenated and deoxygenated blood.
- Use of contrast agents for molecular imaging.

sources: Paul Beard, 2011; Jathoul et al., 2015.

Aim: 3D high-resolution, high sensitivity, quantitative information about physiologically relevant parameters such as chromophore concentration.

- Complete inversion (acoustic + optical + spectral).
- Model-based approaches promising.

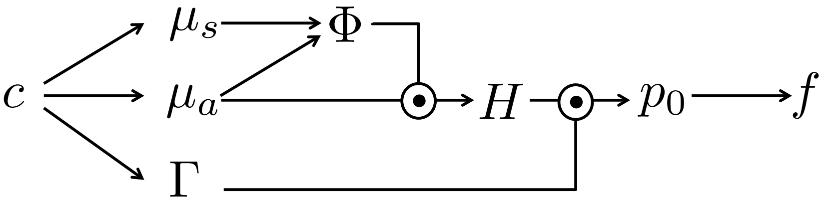

Cox, Laufer, Arridge, Beard, 2011. *Quantitative spectroscopic photoacoustic imaging: a review*, Journal of Biomedical Optics.

Quantitative Photoacoustic Tomography (QPAT)

Aim: 3D high-resolution, high sensitivity, quantitative information about physiologically relevant parameters such as chromophore concentration.

- Complete inversion (acoustic + optical + spectral).
- Model-based approaches promising.

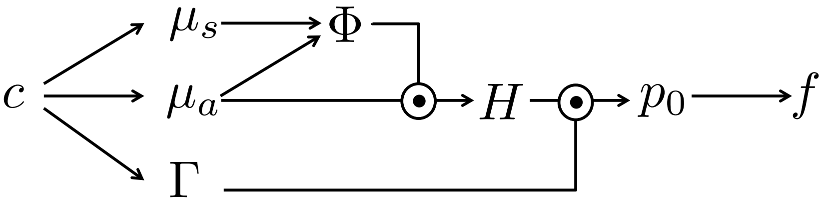

Big gap between simulations and experimental verifications!

Cox, Laufer, Arridge, Beard, 2011. *Quantitative spectroscopic photoacoustic imaging: a review*, Journal of Biomedical Optics.

QPAT Experiment: Overview

1. Phantom development
   - realistic, stable phantom (matching blood, in-vivo environment).
   - characterization of optical, acoustic and thermoelastic properties.
2. Experimental measurements
   - accurate, absolute measurements of acoustic field.
   - measurement of optical excitation parameters.
3. Acoustic reconstruction
   - quantitative, high-res 3D recon of initial acoustic pressure.
4. Optical reconstruction
   - quantitative, high-res 3D recon of chromophore concentrations.

Fonseca, Malone, L, Ellwood, An, L, Arridge, Beard, Cox, 2017. *Three-dimensional photoacoustic imaging and inversion for accurate quantification of chromophore distributions*, Proc. SPIE 2017.

Aim: Similar properties as oxy- and deoxyhemoglobin.

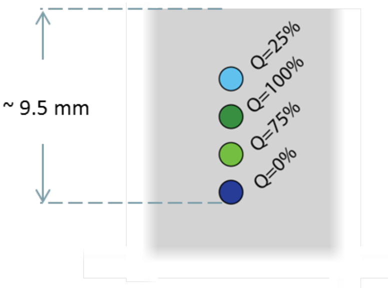

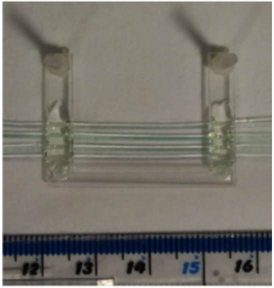

- 4 polythene tubes (580μm inner diameter, 190μm wall thickness).
- copper sulphate ($CuSO_4.5H_2O$) and nickel sulphate ($NiSO_4.6H_2O$): photostable, absorption linear with concentration.
- mixtures with Q % ratio of $NiSO_4.6H_2O$ mother solution.
- background intralipid and india ink solution as scattering medium

Aim: Similar properties as oxy- and deoxyhemoglobin.

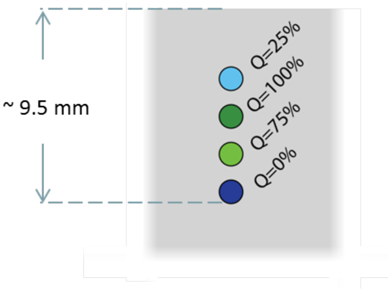

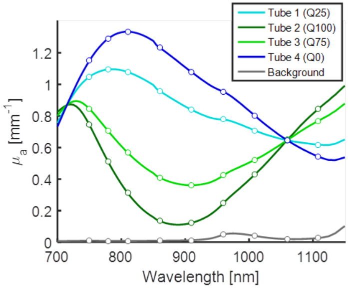

- 4 polythene tubes (580μm inner diameter, 190μm wall thickness).
- copper sulphate ($CuSO_4.5H_2O$) and nickel sulphate ($NiSO_4.6H_2O$): photostable, absorption linear with concentration.
- mixtures with Q % ratio of $NiSO_4.6H_2O$ mother solution.
- background intralipid and india ink solution as scattering medium
- spectra measured with spectrophotometer

Aim: Similar properties as oxy- and deoxyhemoglobin.

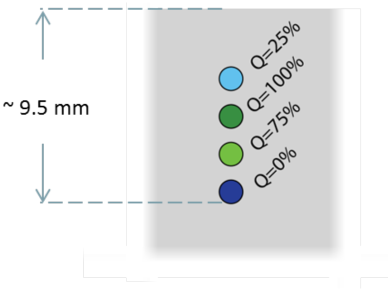

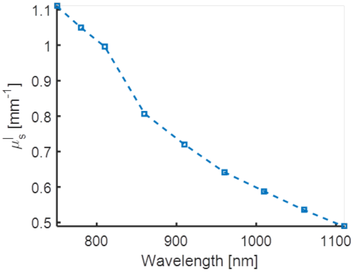

- 4 polythene tubes (580μm inner diameter, 190μm wall thickness).
- copper sulphate ($CuSO_4.5H_2O$) and nickel sulphate ($NiSO_4.6H_2O$): photostable, absorption linear with concentration.
- mixtures with Q % ratio of $NiSO_4.6H_2O$ mother solution.
- background intralipid and india ink solution as scattering medium
- spectra measured with spectrophotometer

The Phantom

Aim: Similar properties as oxy- and deoxyhemoglobin.

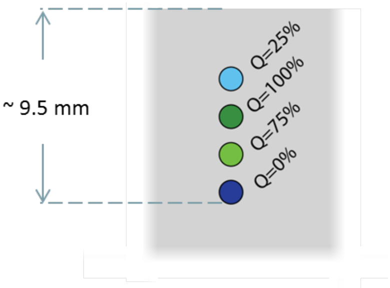

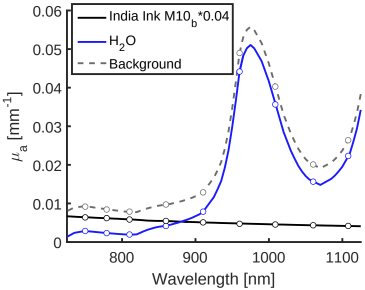

- 4 polythene tubes (580μm inner diameter, 190μm wall thickness).
- copper sulphate ($CuSO_4.5H_2O$) and nickel sulphate ($NiSO_4.6H_2O$): photostable, absorption linear with concentration.
- mixtures with Q % ratio of $NiSO_4.6H_2O$ mother solution.
- background intralipid and india ink solution as scattering medium
- spectra measured with spectrophotometer

Photoacoustic Efficiency / Grüneisenparameter

- $p_0 = \Gamma(c)H$
- Linear dependence found by photoacoustic spectroscopy:

$$\Gamma = \Gamma_{H_2O}\,(1 + \beta_{CuSO_4}\, c_{CuSO_4} + \beta_{NiSO_4}\, c_{NiSO_4}) \qquad \text{(range: } 1 - 1.72\text{)}$$

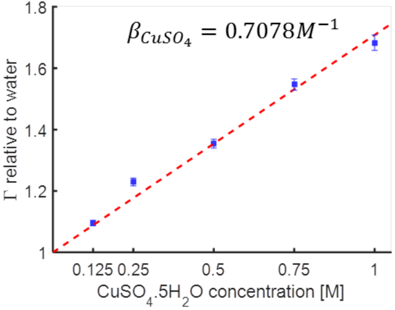

Stahl, Allen, Beard, 2014. *Characterization of the thermalisation efficiency and photostability of photoacoustic contrast agents*, Proc. SPIE.

High Resolution PAT Scanner

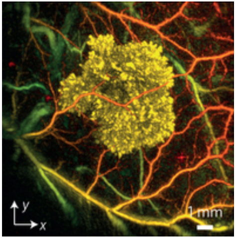

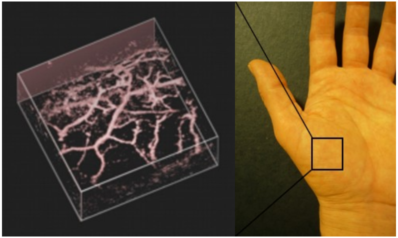

- Fabry-Pérot sensors: wide bandwidth, small element size, low noise, almost omni-directional
- data acquisition gets faster and faster

Ellwood, Ogunlade, Zhang, Beard, Cox, 2017. *Photoacoustic tomography using orthogonal Fabry Pérot sensors*, Journal of Biomedical Optics.

sources: Paul Beard, 2011; Jathoul et al., 2015, Ellwood et al., 2017.

High Resolution PAT Scanner

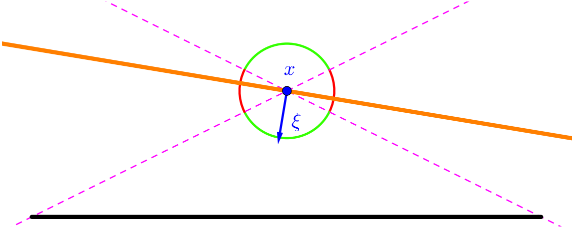

- Fabry-Pérot sensors: wide bandwidth, small element size, low noise, almost omni-directional
- data acquisition gets faster and faster

Ellwood, Ogunlade, Zhang, Beard, Cox, 2017. *Photoacoustic tomography using orthogonal Fabry Pérot sensors*, Journal of Biomedical Optics.

sources: Paul Beard, 2011; Jathoul et al., 2015, Ellwood et al., 2017.

High Resolution PAT Scanner

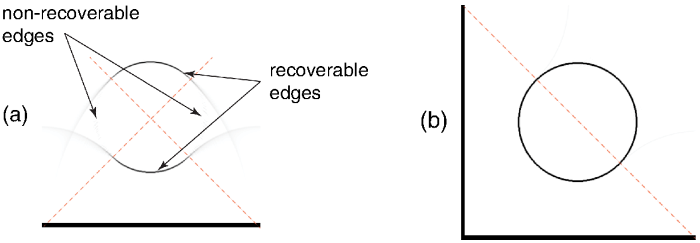

- Fabry-Pérot sensors: wide bandwidth, small element size, low noise, almost omni-directional
- data acquisition gets faster and faster
- two orthogonal sensors to reduce limited view artefacts

Ellwood, Ogunlade, Zhang, Beard, Cox, 2017. *Photoacoustic tomography using orthogonal Fabry Pérot sensors*, Journal of Biomedical Optics.

sources: Paul Beard, 2011; Jathoul et al., 2015, Ellwood et al., 2017.

High Resolution PAT Scanner

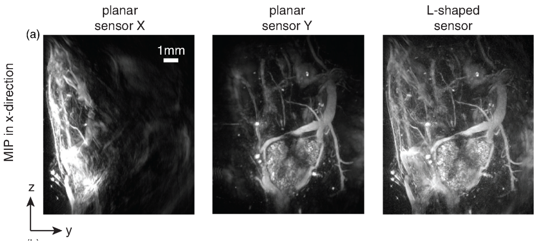

- Fabry-Pérot sensors: wide bandwidth, small element size, low noise, almost omni-directional
- data acquisition gets faster and faster
- two orthogonal sensors to reduce limited view artefacts

Ellwood, Ogunlade, Zhang, Beard, Cox, 2017. *Photoacoustic tomography using orthogonal Fabry Pérot sensors*, Journal of Biomedical Optics.

sources: Paul Beard, 2011; Jathoul et al., 2015, Ellwood et al., 2017.

Experimental Setup

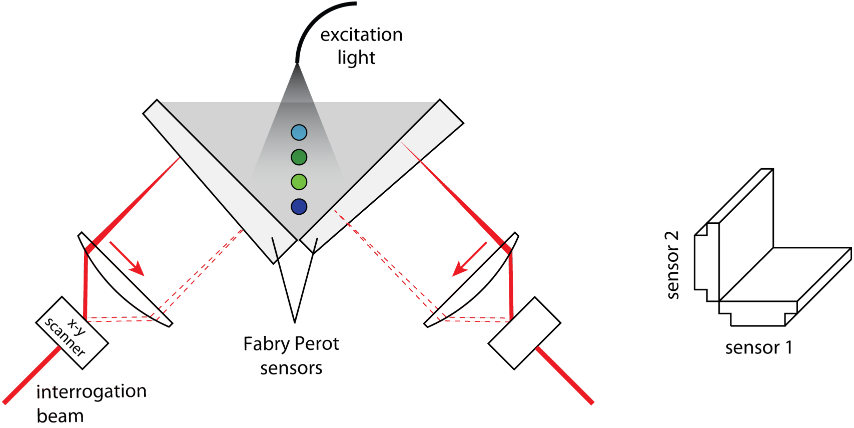

- excitation: 7ns pules at 10Hz with 19mJ at 800nm
- spatial sampling 100μm, temporal sampling: 8ns

Experimental Setup

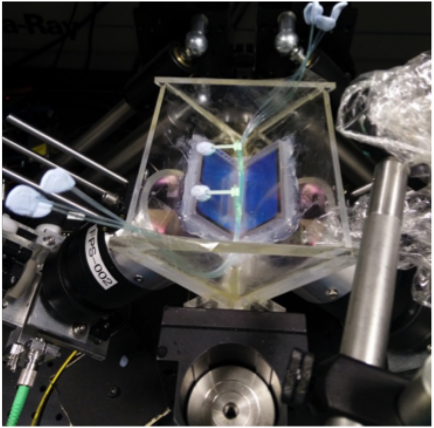

- excitation: 7ns pules at 10Hz with 19mJ at 800nm
- spatial sampling 100μm, temporal sampling: 8ns

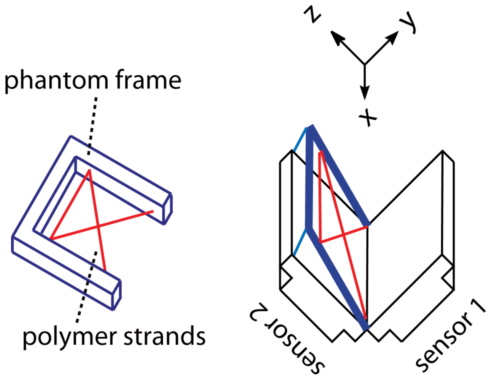

- spatial alignment with registration phantom
- V to Pa conversion by characterisation with calibrated transducer
- Pa corrected for pulse energy variations with integrating sphere

$$f_i(t) = p(y_i, t), \quad \Delta p - \frac{1}{c^2}\frac{\partial^2 p}{\partial^2 t} = 0, \quad p|_{t=0} = p_0, \quad \frac{\partial p}{\partial t}|_{t=0} = 0$$

$$f = A p_0$$

- pre-processing & sound speed calibration
- model-based inversion:

$$\hat{p} = \underset{p \geqslant 0}{\operatorname{argmin}} \|Ap - f\|_2^2$$

via projected gradient-descent-type scheme (iterative time reversal):

$$p^{k+1} = \Pi\left(p^k - A^{\triangleleft}(Ap^k - f)\right)$$

- numerical wave propagation simulation.
- 50μm voxel resolution: $N = 264 \times 358 \times 360$ (up to 400^3!)

Arridge, Betcke, Cox, L, Treeby, 2016. *On the Adjoint Operator in Photoacoustic Tomography*, *Inverse Problems* 32(11).

Acoustic Wave Propagation: Numerical Solution

k-Wave♣ implements a *k*-space pseudospectral method to solve the underlying system of first order conservation laws:

- Compute spatial derivatives in Fourier space: 3D FFTs.
- Modify finite temporal differences by *k*-space operator and use staggered grids for accuracy and robustness.
- Perfectly matched layer to simulate free-space propagation.
- Parallel/GPU computing leads to massive speed-ups.

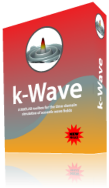

♣ **B. Treeby and B. Cox, 2010**. *k-Wave: MATLAB toolbox for the simulation and reconstruction of photoacoustic wave fields*, *Journal of Biomedical Optics*.

We gratefully acknowledge the support of NVIDIA Corporation with the donation of the Tesla K40 GPU used for this research.

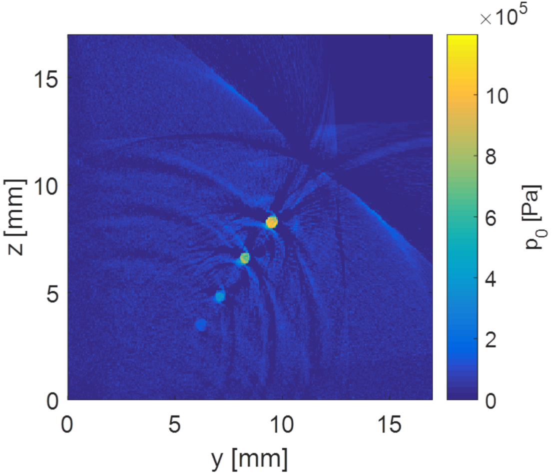

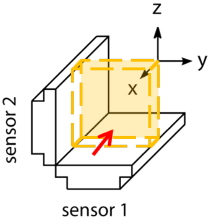

Maximum intensity projection for 1060nm excitation.

Acoustic Inversion Results

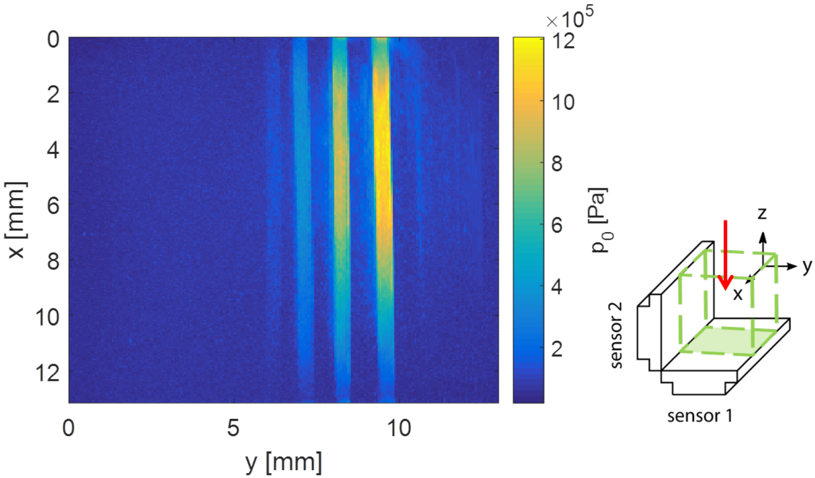

Maximum intensity projection for 1060nm excitation.

Acoustic Inversion Results

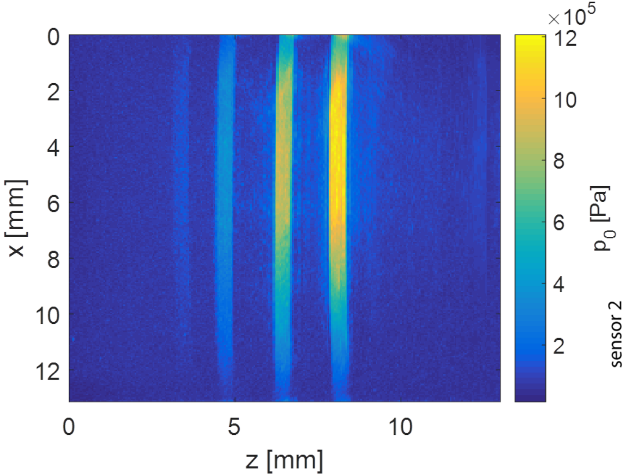

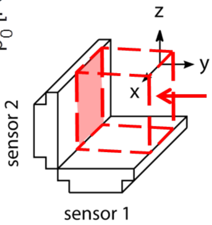

Maximum intensity projection for 1060nm excitation.

Acoustic Inversion Results

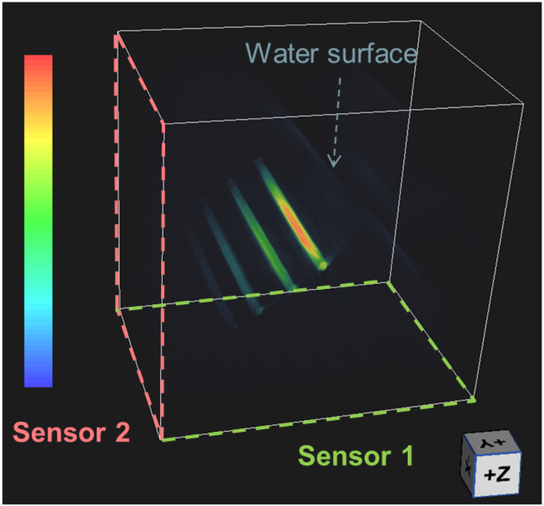

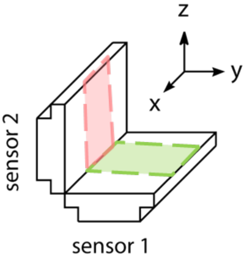

volume rendering for 1060nm excitation.

Acoustic Inversion Results: Different Inversion Approaches

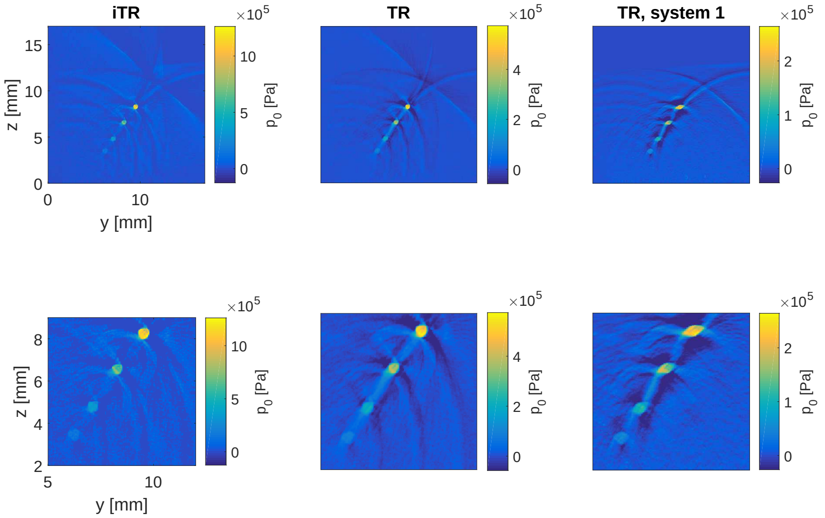

Acoustic Inversion Results: Simulation vs Experiment

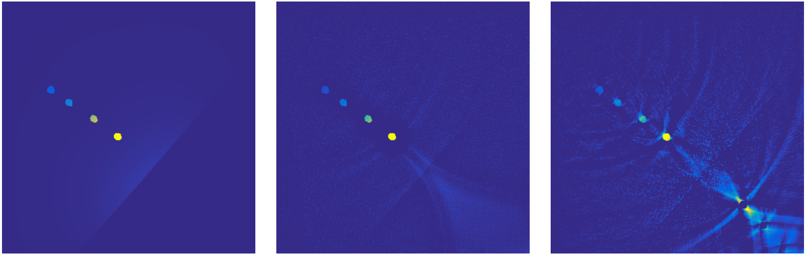

true solution | simulated data recon | experimental data recon

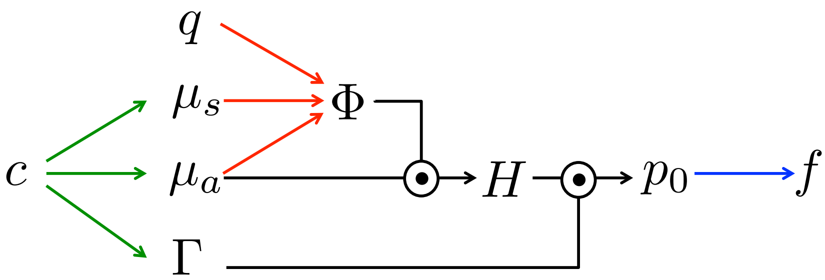

- mapping from c to (μ_a, μ_s, Γ): measured spectra
- q: light source properties
- mapping from (μ_a, μ_s, q) to Φ: non-linear.

Optical Reconstruction: Beam Characterization

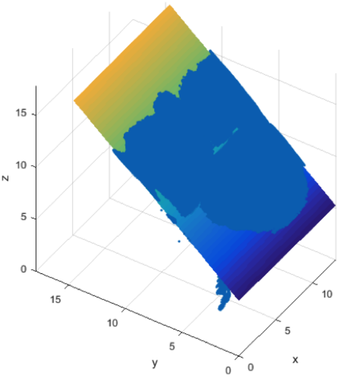

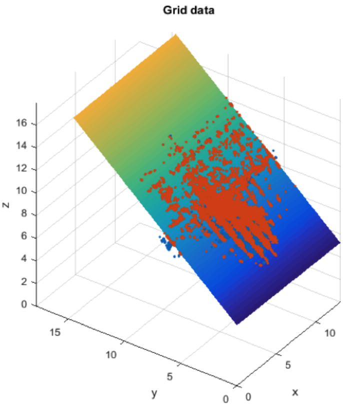

- PA image at water absorption peak to determine surface
- PA image with acetate sheet to determine center and radius

Optical Reconstruction: Beam Characterization

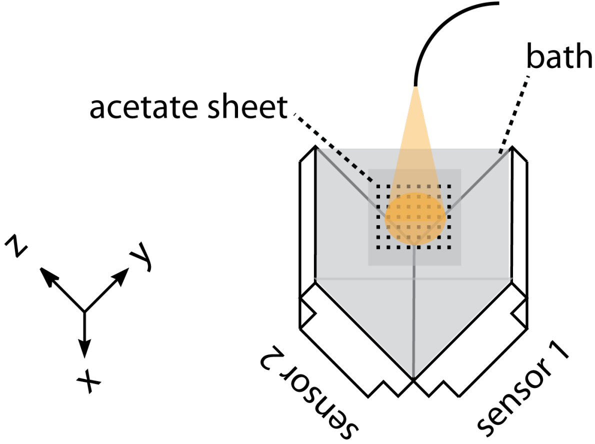

- PA image at water absorption peak to determine surface
- PA image with acetate sheet to determine center and radius

Radiative transfer equation:

$$(s \cdot \nabla + \mu_a + \mu_s)\,\phi(x,s) = q + \mu_s \int \Theta(s,s')\phi(x,s')ds'$$

$$\Phi(x) = \int \phi(x,s)ds$$

! $(x,s) \in \mathbb{R}^5 \rightsquigarrow$ direct FEM infeasible.

Diffusion approximation:

$$(\mu_a - \nabla \cdot \kappa(x)\nabla)\,\Phi(x) = \int q(x,s)ds, \quad \kappa = \frac{1}{3(\mu_a + \mu_s(1-g))}$$

source moved one scattering wave-length into volume.

Toast++:

- time-resolved light transport in highly scattering media
- FEM, different elements and basis functions, 2D and 3D

Schweiger, Arridge, 2014. *The Toast++ software suite for forward and inverse modeling in optical tomography*, *Journal of Biomedical Optics*.

Model Based Inversion

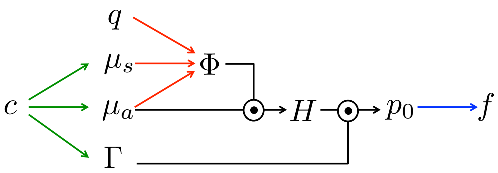

$$\hat{c} = \operatorname*{argmin}_{c \in \mathcal{C}} \sum_{\lambda=1}^{N_\lambda} \int_{ROI} \left(p_{0,\lambda}^{recon} - p_{0,\lambda}(c)\right)^2 dx$$

- solve via iterative first order method (L-BFGS)
- derivatives of $\Phi(\mu_a, \mu_s)$ via adjoint method: two solves of light model per iteration (per wavelength).
- additional data interpolation and rotation into FEM mesh
- addition of global scaling factor.

Malone, Powell, Cox, Arridge, 2015. *Reconstruction-classification method for quantitative photoacoustic tomography*, *JBO.*

Optical Inversion Results

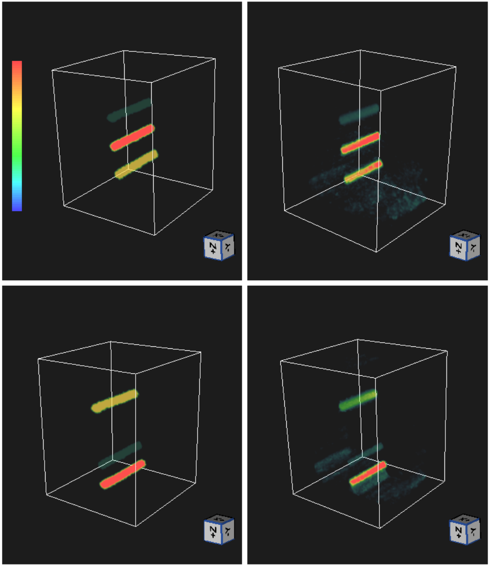

(a)

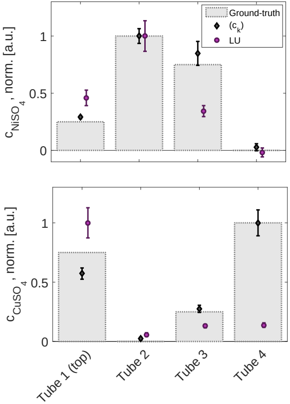

(b)

Optical Inversion Results

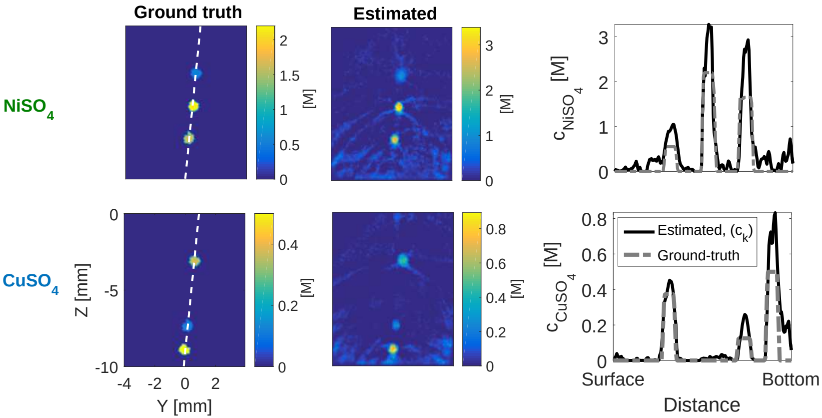

Optical Inversion Results

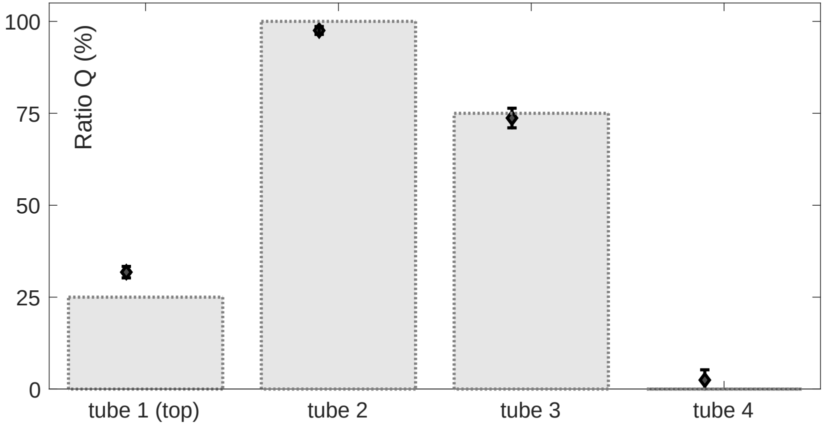

Results for ratio Q, the sO_2 analogue.

$$\delta_{NiSO4} = \frac{\| c_{true}^{(norm)} - c_{est}^{(norm)} \|}{\| c_{true}^{(norm)} \|}$$

Source of explicit uncertainty/error	δ_{NiSO4}
None	6.5%
μ_s: 20% overestimation	7.4%
Grüneisen: $\Gamma = \Gamma_{H_2O}$	39.6%
No acoustic pressure calibration	14.4 %
non-iterative time reversal	26.5%
non-iterative time reversal + sensor 1 only	26.4 %

What we wanted to do:

- highly-res, 3D chromophore distributions from exp. PAT data.
- ratio between two chromophores (sO_2 analogue)

What we learned and achieved:

- promising estimates of normalized chromophore concentrations.
- promising ratio estimates
- sensitivity to in-accuracies

What we need to improve:

- experimental set-up & beam characterization
- acoustic reconstruction
- light model
- coupling of acoustic and optical models
- optimization

Fonseca, Malone, L, Ellwood, An, L, Arridge, Beard, Cox, 2017. *Three-dimensional photoacoustic imaging and inversion for accurate quantification of chromophore distributions*, Proc. SPIE 2017.

Arridge, Betcke, Cox, L, Treeby, 2016. *On the Adjoint Operator in Photoacoustic Tomography*, *Inverse Problems* 32(11).

cmic
Centre for Medical Image Computing

EPSRC
Engineering and Physical Sciences Research Council

NVIDIA

We gratefully acknowledge the support of NVIDIA Corporation with the donation of the Tesla K40 GPU used for this research.

Thank you for your attention!

- **Fonseca, Malone, L, Ellwood, An, L, Arridge, Beard, Cox, 2017**. *Three-dimensional photoacoustic imaging and inversion for accurate quantification of chromophore distributions*, Proc. SPIE 2017.
- **Arridge, Betcke, Cox, L, Treeby, 2016**. *On the Adjoint Operator in Photoacoustic Tomography*, *Inverse Problems* 32(11).

cmic Centre for Medical Image Computing

EPSRC Engineering and Physical Sciences Research Council

NVIDIA

We gratefully acknowledge the support of NVIDIA Corporation with the donation of the Tesla K40 GPU used for this research.